Coordinated Planning of Converter-Based DG Units and Soft Open Points Incorporating Active Management in Unbalanced Distribution Networks

Jian Wang, *Student Member, IEEE*, Niancheng Zhou, *Member, IEEE*,
C.Y. Chung, *Fellow, IEEE*, and Qianggang Wang, *Member, IEEE*

***Abstract*—Soft open points (SOPs) can transfer active power between feeders and compensate reactive power. These features help increase the integration capacity of distributed generation (DG), but the installation location and capacity of SOPs will affect DG planning. In addition, the distribution networks are usually unbalanced due to asymmetric line parameters, unbalanced loads, and DG. Converter-based DG units and SOPs have individual phase active and reactive power regulating ability and provide unbalance compensation. The objective of this paper is to develop a coordinated planning model of converter-based DG units and SOPs in an unbalanced distribution network (UDN) to incorporate their individual phase power control abilities. The individual phase power control characteristics of DG converters and SOPs are first analyzed. A bi-level optimization model of converter-based DG units and SOP planning is then established, in which the upper-level problem minimizes the total cost of the UDN and the lower-level problem minimizes the power loss and voltage unbalance. The bi-level model is transformed into a single-level mixed integer second-order cone programming problem that can be efficiently solved by widely used commercial solvers. Finally, the proposed model is verified on IEEE 33-node and Taiwan Power Company systems.**

***Index Terms*—Unbalanced distribution networks, coordinated planning, distributed generation, soft open points, mixed integer second-order cone programming**

NOMENCLATURE

Indexes	
ϕ	Index for phases and ϕ=A, B and C
i, j	Indexes for nodes
ij	Index for branches
l	Index for scenarios
sub	Index for substations
Parameters	
$A_{i,\mathrm{SOP}}$, $A_{j,\mathrm{SOP}}$	Power loss coefficients of an SOP at node i and j
$c_{\mathrm{I,DG}}$	Investment costs per apparent power of DG
$c_{\mathrm{I,SOP}}$	Investment costs per apparent power of SOP
$c_{\mathrm{O,DG}}$	Operation costs per kWh of DG
c_{P}	Purchase cost per kWh
$C_{\mathrm{I,DG}}$	DG investment cost
$C_{\mathrm{I,SOP}}$	SOP investment cost
$C_{\mathrm{O,DG}}$	DG operation cost
$C_{\mathrm{O,SOP}}$	SOP operation cost
C_{P}	Electricity purchase cost
CH	Calinski-Harabasz index
d	Discount rate
$e^r_{i,\phi}$, $f^r_{i,\phi}$	Real and imaginary parts of the rated voltage of phase-ϕ at node i
$I^{\max}_{ij,\phi}$	Maximum branch current of phase-ϕ of branch ij
k	Number of clusters
K_T	Total scenario number
m_i, n_{ij}	Length of binary variables
n_b	Total node number
n_{SOP}	Total SOP number
n_l	Total branches number
$P^{l,\max}_{i,\phi\mathrm{DG}}$	Maximum active power of phase-ϕ at node i in scenario l of DG
p^l	Ratio of active power generation of DG to its capacity
$\tilde{P}_{i,\phi}$, $\tilde{Q}_{i,\phi}$, $\tilde{P}_{\mathrm{sub},\phi}$, $\tilde{Q}_{\mathrm{sub},\phi}$	Constants in the power flow equations
$r_{ij,\phi}$	Resistance of phase-ϕ of branch ij
$S^{\max}_{i,\mathrm{DG}}$	Maximum allowable installation capacities of the DG at node i
$S^{\max}_{ij,\mathrm{SOP}}$	Maximum allowable installation capacities of the SOPs at branch ij
s_{DG}	Unit capacity of the DG
s_{SOP}	Unit capacity of the SOPs
S_{sub}	Capacity of the substation transformer
T^l	Total hours of scenario l
T_{an}	Total hours for one year
$U^{\min}$, $U^{\max}$	Minimum and maximum node voltage
$U^r_{i,\phi}$	Rated voltage of phase-ϕ at node i
$y_{i,\phi j,\phi'}$	Element in the nodal admittance matrix
y	Lifetime of the DG and SOPs
$z_{ij,\phi}$	Modulus of impedance of phase-ϕ of branch ij
α	Coefficient of the annual operation costs of SOP
$\varsigma^{\min}$, $\varsigma^{\max}$	Minimum and maximum coefficients of

This work was supported by the National Key Research and Development Program of China (2018YFB0904604), the National Natural Science Foundation of China (51877017), the Fundamental Research Funds for the Central Universities (2019CDXYDQ0010), the Chongqing Research Program of Basic Research and Frontier Technology (cstc2016jcyjA0402), and the China Scholarship Council.

J. Wang, N. Zhou, and Q. Wang are with the State Key Laboratory of Power Transmission Equipment and System Security and New Technology, Chongqing University, Chongqing, 400044, China.

C.Y. Chung is with the Department of Electrical and Computer Engineering, University of Saskatchewan, Saskatoon, SK S7N 5A9, Canada.

	reactive power generation of DG
$\xi^{\min}, \xi^{\max}$	Minimum and maximum coefficients of reactive power injection of an SOP
ω_1, ω_2, ω_3	Weighting coefficients of the sub-functions in the lower-level problem model
$\Re_{j,\phi'}^{p,i,\phi}$, $\Im_{j,\phi'}^{p,i,\phi}$	Coefficients of the real and imaginary parts of the node voltage of the active power equation
$\Re_{j,\phi'}^{q,i,\phi}$, $\Im_{j,\phi'}^{q,i,\phi}$	Coefficients of the real and imaginary parts of the node voltage of the reactive power equation
$\Re_{j,\phi'}^{p,\mathrm{sub},\phi}$, $\Im_{j,\phi'}^{p,\mathrm{sub},\phi}$	Coefficients of the real and imaginary parts of the node voltage of the active power equation in the substation
$\Re_{j,\phi'}^{q,\mathrm{sub},\phi}$, $\Im_{j,\phi'}^{q,\mathrm{sub},\phi}$	Coefficients of the real and imaginary parts of the node voltage of the reactive power equation in the substation
Variables	
$a_{1,i}$, $a_{2,i}$, …, $a_{mi,i}$	Dummy binary variables for the number of DG units
$b_{1,ij}$, $b_{2,ij}$, …, $b_{nij,ij}$	Dummy binary variables for the number of SOP units
$e_{i,\phi}^{l}$, $f_{i,\phi}^{l}$	Real and imaginary parts of the voltage of phase-ϕ at node i in scenario l
$e_{i,\mathrm{un}}^{l}$, $f_{i,\mathrm{un}}^{l}$	Real and imaginary parts of the negative sequence component of the voltage at node i in scenario l
f_{line}, f_{SOP}, f_{U}	Square root of line power loss, SOP power loss, and voltage negative sequence unbalance
$I_{i,\phi}^{l}$	Current injection of phase-ϕ at node i in scenario l
$I_{ij,\phi}^{l}$	Branch current of phase-ϕ of branch ij in scenario l
$P_{i,\phi}^{l}$, $Q_{i,\phi}^{l}$	Active and reactive power injection of phase-ϕ at node i in scenario l
$P_{i,\phi,\mathrm{Load}}^{l}$, $Q_{i,\phi,\mathrm{Load}}^{l}$	Active and reactive power consumption of phase-ϕ at node i in scenario l
$P_{\mathrm{sub},\phi}^{l}$, $Q_{\mathrm{sub},\phi}^{l}$	Active and reactive power injection of phase-ϕ in the substation in scenario l
$P_{i,\phi,\mathrm{DG}}^{l}$, $Q_{i,\phi,\mathrm{DG}}^{l}$	Active and reactive power generation of phase-ϕ of DG at node i in scenario l
$P_{i,\phi,\mathrm{SOP}}^{l}$, $Q_{i,\phi,\mathrm{SOP}}^{l}$	Active and reactive power injection of phase-ϕ of an SOP at node i in scenario l
$P_{i,\phi,\mathrm{SOP}}^{\mathrm{L},l}$, $P_{j,\phi,\mathrm{SOP}}^{\mathrm{L},l}$	Power loss of the two converters of an SOP at node i and j
$Q_{i,\phi,\mathrm{DG}}^{\min}$, $Q_{i,\phi,\mathrm{DG}}^{\max}$	Minimum and maximum reactive power generation of phase-ϕ of DG at node i
$Q_{i,\phi,\mathrm{SOP}}^{\min}$, $Q_{i,\phi,\mathrm{SOP}}^{\max}$	Minimum and maximum reactive power injection of phase-ϕ of an SOP at branch ij
$S_{i,\phi,\mathrm{DG}}$, $S_{i,3\phi,\mathrm{DG}}$	Phase-ϕ capacity and total capacity of DG at node i
$U_{i,\phi}^{l}$	Voltage of phase-ϕ at node i in scenario l
$y_{i,\mathrm{DG}}$	Number of DG units
$y_{ij,\mathrm{SOP}}$	Number of SOP units

I. Introduction

Distributed generation (DG) has technical advantages (e.g., loss reduction, improving voltage profile) and is also environmentally friendly [1], and as such the integration of DG is receiving increasing attention. However, crude decisions with respect to DG planning cannot maximize the benefits. Regulators are gradually pushing power utilities to develop reasonable strategies to choose the optimal location and capacity of DG units [2, 3]. The installation of DG units is constrained by geographic location and safe operation. Increasing the installation capacity of DG units will violate the upper limit of voltage, which limits their further integration [4]. Soft open points (SOPs) are a type of power electronic equipment that is replacing the traditional normally open switch. SOPs are connected between feeders by two back-to-back voltage source converters (VSCs), which can transfer active power and compensate the reactive power [5, 6]. These features can help increase the integration capacity of DG. The location and capacity of SOPs affects the power transfer between the feeders, and thus the capacity of DG. Therefore, installations of DG and SOPs should be planned together.

In addition, asymmetric line parameters, unbalanced loads, and DG resources cause voltage imbalances in distribution networks [7]. Unbalanced voltage not only increases the power loss but also affects the normal operation of power equipment [8]. Fortunately, the active and reactive power of each phase of a DG converter and SOP can be controlled independently [9] and this control characteristic can help to improve load unbalance in an unbalanced distribution network (UDN). The coordinated planning of DG converters and SOPs in UDNs should be investigated to incorporate their individual phase power control abilities.

Previous research on DG and SOP planning problems mainly focused on symmetrical distribution networks, in which the power and line parameters of each phase are the same [10-16]. Some works propose the optimal planning of DG unit locations [10] and model the allocation of DG and reactive power [11]. DG planning models considering distribution network reconfiguration and the operation and power control of photovoltaic inverters are proposed in [12-14]. SOP planning, siting, and sizing in distribution networks is studied in [15], and coordinated allocation of DG, capacitor banks, and SOPs is proposed in [16]. A few research achievements have been made with respect to DG planning in UDNs [3, 17]. The optimal placement and sizing of DG units in UDNs is studied in [17], but the impact on the unbalance is not analyzed. The placement and sizing of inverter-based DG units in UDNs considering the active power curtailment and reactive power support of DG are considered in [3]. However, this optimization model only considers investment and operation costs and ignores the influence on power loss and unbalance. In addition, the effect of loss reduction and unbalance compensation relying on DG alone is limited. Hence, the operation of DG and SOPs in UDNs should also be considered to reduce power loss and voltage unbalance.

Bi-level optimization is an appropriate method to deal with the optimal planning problem of DG and SOPs and considering active network management. The upper-level

problem determines the location and capacity of DG and SOPs, while the lower-level model concerns the optimal operation control of the UDNs. Solution methods for bi-level optimization mainly include the iterative algorithm [16] and single-level problem conversion based on dual theory or the Karush–Kuhn–Tucker (KKT) conditions [18]. From a mathematical point of view, the transformation methods for a single-level optimization model based on a dual model or KKT conditions are the same [19]. The iterative algorithm has low efficiency. It is also difficult to obtain the optimal solution of the optimization problem based on the iterative algorithm because the lower-level model involves nonlinear constraints such as the three-phase power flow equation. The solution efficiency can be improved by converting the bi-level model to a single-level programming model, but this method requires strong duality of the lower-level model. Therefore, this nonlinear programming (NLP) lower-level model should be transformed into a convex model with strong duality. Second-order cone programming (SOCP) is a convex optimization model with good convergence and efficiency [20] that has been widely used in optimal power flow, operation, and planning of distribution systems. However, the existing SOCP model uses a variable to replace the voltage square, so the voltage phase information and voltage unbalance for a three-phase distribution system cannot be obtained.

To address this research gap, this paper proposes a mixed integer SOCP (MISOCP) model for the optimal planning of DG units and SOPs incorporating the active management of the converter in UDNs. The main contributions of this paper can be summarized as follows:

1) Individual phase power control characteristics of DG converters and SOPs are analyzed, and their active and reactive power regulating regions are constructed. Then, a bi-level optimization model for DG and SOP planning in UDNs is proposed with consideration of their regulating abilities. The upper-level problem is to minimize the total cost of the UDN while the lower-level problem aims to minimize the power loss and voltage unbalance.

2) To improve the convergence and efficiency, the lower-level problem is transformed into an SOCP model through three-phase power flow equation linearization and second-order cone (SOC) relaxation. The model is not only convex, but also retains voltage phase information. Then, the bi-level model is transformed into a single-level MISOCP model by Lagrange duality theory and the big-M method.

3) The effectiveness of the proposed model is verified on an IEEE 33-node system and the Taiwan Power Company (TPC) system [21, 22].

The remainder of this paper is organized as follows. In Section II, the individual phase power control characteristics of DG converters and SOPs are analyzed. The bi-level planning model of DG and SOPs is established in Section III. In Section IV, the bi-level optimization model is converted to a single-level MISOCP problem. In Section V, case studies are presented. Conclusions are drawn in Section VI.

II. Individual Phase Power Control Characteristics of DG Converters and SOPs

Fig. 1 shows the control principle of DG converters and SOPs with individual phase power control. As shown in Fig. 1(a), DG access to a UDN is through power electronics that have excellent controllability and flexible power regulation ability. In the PQ control mode, the DG converter controls the active and reactive power of each phase $P_{\phi,\mathrm{DG}}$, $Q_{\phi,\mathrm{DG}}$ (ϕ = A, B, C) on the AC side of the converter through the VSC controller according to feedback of the AC side current $I_{\phi,\mathrm{DG}}$ and voltage $U_{\phi,\mathrm{DG}}$ in the closed-loop control structure [23]. The SOP based on VSCs in Fig. 1 (b) also has similar characteristics as well as a power flow transfer function. There are two VSCs in an SOP, one of which adopts PQ control mode and the other adopts V_{dc}Q control mode. The VSC with PQ control is used to control the transmitted active power $P_{\phi,\mathrm{SOP}}$ of the SOP and the reactive power injected by the converter, while the VSC with V_{dc}Q control is used to maintain the voltage constant of the DC bus and inject reactive power [6]. The active and reactive power of each phase can be controlled independently by the VSC controller in a UDN.

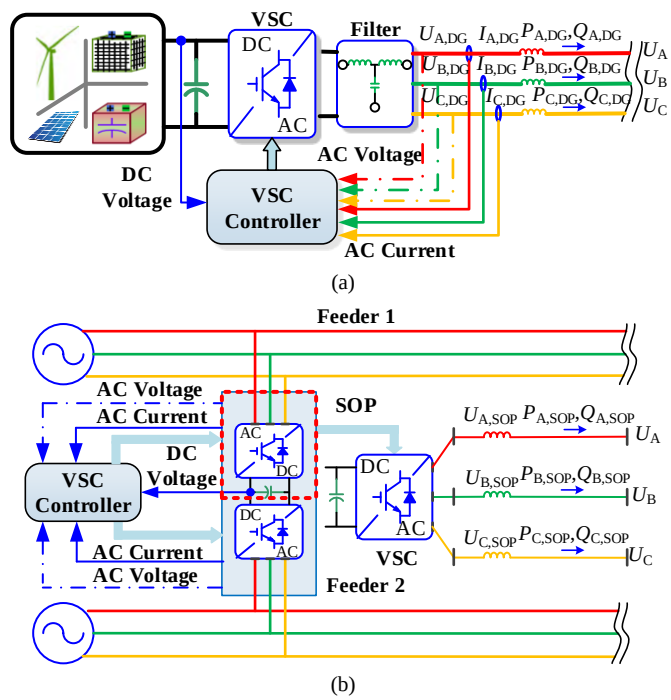

Fig. 1 Schematic of (a) DG converters and (b) SOPs with respect to individual phase power control.

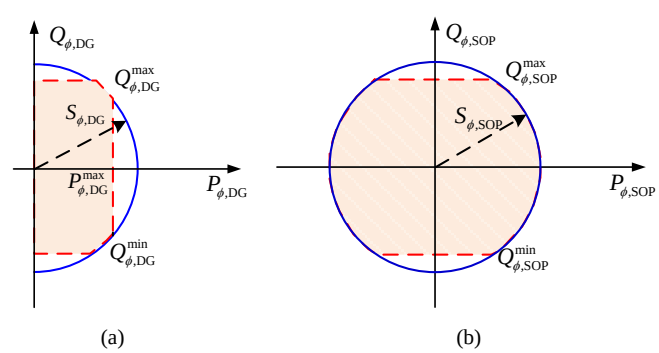

Fig. 2 Active and reactive power regulating region: (a) DG; (b) SOP.

The reactive power of DG, $Q_{\phi,\mathrm{DG}}$, should be within the

constraint range [$Q_{\phi,\mathrm{DG}}^{\min}$, $Q_{\phi,\mathrm{DG}}^{\max}$] considering its safe operation [24]. Similarly, the reactive power of an SOP should be located in the interval [$Q_{\phi,\mathrm{SOP}}^{\min}$, $Q_{\phi,\mathrm{SOP}}^{\max}$]. The active power of DG, $P_{\phi,\mathrm{DG}}$, cannot exceed the rated active power, $P_{\phi,\mathrm{DG}}^{\max}$. In addition, the apparent power of each phase of both DG and an SOP should be less than their respective capacities, $S_{\phi,\mathrm{DG}}$ and $S_{\phi,\mathrm{SOP}}$. Therefore, based on the above analysis, the active and reactive power regulating region of DG units and SOPs are shown in Fig. 2. According to the clustering method and annual hourly load demand and DG output data, multiple scenarios are constructed to represent the stochastic behavior of load demand and DG generation in Section III-C. These two regions for scenario l can also be represented by (1) -(3) and (4) -(10), respectively.

$$\begin{aligned} &0 \le P_{i,\phi,\mathrm{DG}}^{l} \le P_{i,\phi,\mathrm{DG}}^{l,\max} \\ &P_{i,\phi,\mathrm{DG}}^{l,\max} = p^{l} S_{i,\phi,\mathrm{DG}} \end{aligned} \tag{1}$$

$$\begin{cases} Q_{i,\phi,\mathrm{DG}}^{\min} \le Q_{i,\phi,\mathrm{DG}}^{l} \le Q_{i,\phi,\mathrm{DG}}^{\max} \\ Q_{i,\phi,\mathrm{DG}}^{\min} = \varsigma^{\min} S_{i,\phi,\mathrm{DG}}\ ;\ Q_{i,\phi,\mathrm{DG}}^{\max} = \varsigma^{\max} S_{i,\phi,\mathrm{DG}};\ S_{i,\phi,\mathrm{DG}} = S_{i,3\phi,\mathrm{DG}} / 3 \end{cases} \tag{2}$$

$$\sqrt{{P_{i,\phi,\mathrm{DG}}^{l}}^{2} + {Q_{i,\phi,\mathrm{DG}}^{l}}^{2}} \le S_{i,\phi,\mathrm{DG}} \tag{3}$$

Constraints (1), (2), and (3) are active power, reactive power, and DG capacity constraints, respectively.

$$P_{i,\phi,\mathrm{SOP}}^{l} + P_{j,\phi,\mathrm{SOP}}^{l} + P_{i,\phi,\mathrm{SOP}}^{\mathrm{L},l} + P_{j,\phi,\mathrm{SOP}}^{\mathrm{L},l} = 0 \tag{4}$$

$$P_{i,\phi,\mathrm{SOP}}^{\mathrm{L},l} = A_{i,\mathrm{SOP}} \sqrt{{P_{i,\phi,\mathrm{SOP}}^{l}}^{2} + {Q_{i,\phi,\mathrm{SOP}}^{l}}^{2}} \tag{5}$$

$$P_{j,\phi,\mathrm{SOP}}^{\mathrm{L},l} = A_{j,\mathrm{SOP}} \sqrt{{P_{j,\phi,\mathrm{SOP}}^{l}}^{2} + {Q_{j,\phi,\mathrm{SOP}}^{l}}^{2}} \tag{6}$$

$$\begin{cases} Q_{i,\phi,\mathrm{SOP}}^{\min} \le Q_{i,\phi,\mathrm{SOP}}^{l} \le Q_{i,\phi,\mathrm{SOP}}^{\max} \\ Q_{i,\phi,\mathrm{SOP}}^{\min} = \xi^{\min} S_{ij,\phi,\mathrm{SOP}};\ Q_{i,\phi,\mathrm{SOP}}^{\max} = \xi^{\max} S_{ij,\phi,\mathrm{SOP}};\ S_{ij,\phi,\mathrm{SOP}} = S_{ij,3\phi,\mathrm{SOP}} / 3 \end{cases} \tag{7}$$

$$\begin{cases} Q_{j,\phi,\mathrm{SOP}}^{\min} \le Q_{j,\phi,\mathrm{SOP}}^{l} \le Q_{j,\phi,\mathrm{SOP}}^{\max} \\ Q_{j,\phi,\mathrm{SOP}}^{\min} = \xi^{\min} S_{ij,\phi,\mathrm{SOP}};\ Q_{j,\phi,\mathrm{SOP}}^{\max} = \xi^{\max} S_{ij,\phi,\mathrm{SOP}};\ S_{ij,\phi,\mathrm{SOP}} = S_{ij,3\phi,\mathrm{SOP}} / 3 \end{cases} \tag{8}$$

$$\sqrt{{P_{i,\phi,\mathrm{SOP}}^{l}}^{2} + Q_{i,\phi,\mathrm{SOP}}^{l}} \le S_{ij,\phi,\mathrm{SOP}} \tag{9}$$

$$\sqrt{{P_{j,\phi,\mathrm{SOP}}^{l}}^{2} + Q_{j,\phi,\mathrm{SOP}}^{l}} \le S_{ij,\phi,\mathrm{SOP}} \tag{10}$$

Constraint (4) is the active power balance of an SOP [25]. Constraints (5) and (6) define the power loss equation of an SOP [25]. Constraints (7) and (8) are the reactive power constraints of an SOP. Constraints (9) and (10) are the SOP capacity constraints.

III. Bi-level Planning Model

The planning related to DG and SOPs proposed in this paper adopts bi-level optimization. This model not only includes the investment and operational costs of DG and SOPs, but also the effect of individual power control characteristics of DG converters and SOPs on power loss and unbalance.

A. Upper-level Problem

The objective of the upper-level problem is to minimize the total annual costs C.

$$\min_{\boldsymbol{x}_{\mathrm{UL}}} C = C_{\mathrm{I,DG}} + C_{\mathrm{I,SOP}} + C_{\mathrm{O,DG}} + C_{\mathrm{O,SOP}} + C_{\mathrm{P}} \tag{11}$$

$$C_{\mathrm{I,DG}} = \frac{d(1+d)^{y}}{(1+d)^{y}-1} \sum_{i=1}^{n_b} c_{\mathrm{I,DG}} S_{i,3\phi,\mathrm{DG}} \tag{12}$$

$$C_{\mathrm{I,SOP}} = \frac{d(1+d)^{y}}{(1+d)^{y}-1} \sum_{ij \in n_{\mathrm{SOP}}} c_{\mathrm{I,SOP}} S_{ij,3\phi,\mathrm{SOP}} \tag{13}$$

$$C_{\mathrm{O,DG}} = c_{\mathrm{O,DG}} \sum_{i=1}^{n_b} \sum_{\phi=\mathrm{A,B,C}} \sum_{k=1}^{K_T} P_{i,\phi,\mathrm{DG}}^{l} T^{l} \tag{14}$$

$$C_{\mathrm{O,SOP}} = \alpha \sum_{ij \in n_{\mathrm{SOP}}} c_{\mathrm{I,SOP}} S_{ij,3\phi,\mathrm{SOP}} \tag{15}$$

$$C_{\mathrm{P}} = c_{\mathrm{P}} \sum_{l=1}^{K_T} \sum_{\phi=\mathrm{A,B,C}} P_{\mathrm{sub},\phi}^{l} T^{l} \tag{16}$$

s.t.

$$S_{i,3\phi,\mathrm{DG}} \le S_{i,\mathrm{DG}}^{\max} \tag{17}$$

$$\begin{cases} S_{i,3\phi,\mathrm{DG}} = y_{i,\mathrm{DG}} s_{\mathrm{DG}} \\ y_{i,\mathrm{DG}} = a_{1,i} + 2 \cdot a_{2,i} + \cdots + 2^{m_i - 1} \cdot a_{m_i,i} \\ m_i = \left\lceil \log_2^{S_{i,\mathrm{DG}}^{\max} / s_{\mathrm{DG}} + 1} \right\rceil \end{cases} \tag{18}$$

$$S_{ij,3\phi,\mathrm{SOP}} \le S_{ij,\mathrm{SOP}}^{\max} \tag{19}$$

$$\begin{cases} S_{ij,3\phi,\mathrm{SOP}} = y_{ij,\mathrm{SOP}} s_{\mathrm{SOP}} \\ y_{ij,\mathrm{SOP}} = b_{1,ij} + 2 \cdot b_{2,ij} + \cdots + 2^{n_{ij} - 1} \cdot b_{n_{ij},ij} \\ n_{ij} = \left\lceil \log_2^{S_{ij,\mathrm{SOP}}^{\max} / s_{\mathrm{SOP}} + 1} \right\rceil \end{cases} \tag{20}$$

where variable $\boldsymbol{x}_{\mathrm{UL}} = \{a_{1,i}, a_{2,i}, \ldots, a_{mi,i}, b_{1,ij}, b_{2,ij}, \ldots, b_{nij,ij}\}$. T^{l} is equal to the sample number of cluster l. (12) and (13) are the annual investment cost of DG and SOPs, respectively, considering the discount rate and their lifetime [26]. (14) and (15) are the annual operation costs of DG and SOPs, respectively. (16) is the annual electricity purchase cost from the upstream grid. Constraints (17) and (19) are the capacity limits of DG and SOPs, respectively. In constraints (18) and (20), the relation equations between installation capacity and binary variables are provided. For simplicity, we assume that all DG or SOP units have the same capacity. The installation capacities at different locations are determined based on the number of units, and this assumption does not affect the planning results. The number of DG units $y_{i,\mathrm{DG}}$ can be represented by dummy binary variables $a_{1,i}, a_{2,i}, \ldots, a_{mi,i}$. $\lceil \cdot \rceil$ is a ceiling function and m_i is the length of binary variables. Therefore, the range of DG unit numbers is 0 ~ (2^{mi}-1). Similarly, the number of SOP units is between 0 and (2^{nij}-1).

B. Lower-level Problem

The lower-level problem is to minimize the power loss and voltage negative sequence unbalance.

$$\min_{\boldsymbol{x}_{\mathrm{PLL}}} F_{\mathrm{PLL}} = \omega_1 f_{\mathrm{line}} + \omega_2 f_{\mathrm{SOP}} + \omega_3 f_{\mathrm{U}} \tag{21}$$

s.t.

$$f_{\mathrm{line}}^{2} = \sum_{ij \in n_l} \sum_{\phi=\mathrm{A,B,C}} \sum_{l=1}^{K_T} {I_{ij,\phi}^{l}}^{2} r_{ij,\phi} T^{l} / T_{\mathrm{an}} \tag{22}$$

$$f_{\mathrm{SOP}} = \sum_{ij \in n_{\mathrm{SOP}}} \sum_{\phi=\mathrm{A,B,C}} \sum_{l=1}^{K_T} \left(P_{i,\phi,\mathrm{SOP}}^{\mathrm{L},l} + P_{j,\phi,\mathrm{SOP}}^{\mathrm{L},l} \right) T^{l} / T_{\mathrm{an}} \tag{23}$$

$$f_{\mathrm{U}} = \sqrt{\sum_{i=1}^{n_b} \sum_{l=1}^{K_T} \left(\dot{U}_{i,\mathrm{A}}^{l} / 3 + e^{\mathrm{j}4\pi/3} \dot{U}_{i,\mathrm{B}}^{l} / 3 + e^{\mathrm{j}2\pi/3} \dot{U}_{i,\mathrm{C}}^{l} / 3 \right)^{2} T^{l} / T_{\mathrm{an}}} \tag{24}$$

$$P_{i,\phi}^{l} = P_{i,\phi,\mathrm{DG}}^{l} + P_{i,\phi,\mathrm{SOP}}^{l} - P_{i,\phi,\mathrm{Load}}^{l} \tag{25}$$

$$Q_{i,\phi}^{l} = Q_{i,\phi,\mathrm{DG}}^{l} + Q_{i,\phi,\mathrm{SOP}}^{l} - Q_{i,\phi,\mathrm{Load}}^{l} \tag{26}$$

$$P_{i,\phi}^{l}+\mathrm{j}\cdot Q_{i,\phi}^{l}=\dot{U}_{i,\phi}^{l}\dot{I}_{i,\phi}^{l\,*} \tag{27}$$

$$U^{\min}\le U_{i,\phi}^{l}\le U^{\max} \tag{28}$$

$$\sqrt{{P_{\mathrm{sub},\phi}^{l}}^{2}+{Q_{\mathrm{sub},\phi}^{l}}^{2}}\le S_{\mathrm{sub}}/3 \tag{29}$$

$$I_{ij,\phi}^{l}=\left|\dot{U}_{i,\phi}^{l}-\dot{U}_{j,\phi}^{l}\right|/z_{ij,\phi}\le I_{ij,\phi}^{\max} \tag{30}$$

where variable $\boldsymbol{x}_{\mathrm{PLL}}$ = { f_{line} , f_{SOP} , f_{U} , $P_{i,\phi,\mathrm{DG}}^{l}$, $Q_{i,\phi,\mathrm{DG}}^{l}$, $P_{i,\phi,\mathrm{SOP}}^{l}$, $Q_{i,\phi,\mathrm{SOP}}^{l}$, $P_{i,\phi,\mathrm{SOP}}^{\mathrm{L},l}$, $P_{j,\phi,\mathrm{SOP}}^{\mathrm{L},l}$, $U_{i,\phi}^{l}$, $I_{i,\phi}^{l}$, $P_{i,\phi}^{l}$, $Q_{i,\phi}^{l}$ }. Total hours for a year T_{an}=8760. To facilitate conic relaxation, the square root of line loss f_{line} is used to represent line loss in the objective function.

The linear weighting method is used to transform the multi-objective optimization problem into a single-objective model [25]. The weighting coefficients ω_1, ω_2, and ω_3 are determined via the analytic hierarchy process (AHP) [25, 27]. AHP is a method that combines qualitative and quantitative analysis. The decision-maker first defines the importance between sub-objective functions based on operation experience, and then establishes a pairwise comparison matrix. Finally, weights are calculated according to the comparison matrix. The detailed process can be obtained from [27].

The lower-level problem is composed of an objective function (21), constraints (22)-(30), and DG and SOP constraints (1)-(10). (25) and (26) are respectively the node active and reactive power balance. (27) is the node power constraint. Constraints (28), (29), and (30) are node voltage, substation transformer capacity, and branch current limits, respectively.

C. Scenario Construction

The renewable energy power generation and load are uncertainties for the optimization problem. An optimal planning model based on various scenarios is a common method to compare scenarios; however, substantial computing time is required if all scenarios are considered. Therefore, it is necessary to reduce the number of scenarios while maintaining the characteristics of the original data. In this paper, *k*-means clustering is used to group data samples and reduce the number of scenarios according to data similarity [28]. In general, data similarity in the same cluster is high while in different clusters is low. The clustering procedure is as follows.

Step 1: Select *k* samples randomly as the initial cluster centroids from statistics of the historical hourly renewable energy power generation and load $\{\boldsymbol{g}_1, \boldsymbol{g}_2, \ldots, \boldsymbol{g}_T\}$. $\boldsymbol{g}_i$ (i=1,2, …, T) is a two-dimensional vector and represents the active power of renewable energy and load. The cluster centroids are $\{\boldsymbol{\eta}_1, \boldsymbol{\eta}_2,\ldots, \boldsymbol{\eta}_k\}$.

Step 2: Calculate the Euclidean distance $d_{E,ij}=\|\boldsymbol{g}_i-\boldsymbol{\eta}_j\|_2$ between sample $\boldsymbol{g}_i$ and the cluster centroid $\boldsymbol{\eta}_j$ (j=1,2,…k). Then divide sample $\boldsymbol{g}_i$ into the closest cluster j based on $d_{E,ij}$.

Step 3: Calculate the mean value of samples in each cluster as the new cluster centroid.

Step 4: Repeat **Steps** 2 and 3 until the cluster centroid no longer changes, then output the cluster centroid and samples in each cluster.

The final cluster centroid retains the historical data characteristics of renewable energy generation power and load, which can be regarded as representative sample data. However, the number of clusters k directly affects the clustering result, where k is an integer within the range of [2, $\sqrt{T_{\mathrm{an}}}$] [29]. The Calinski-Harabasz index reflects the dispersion between different clusters and the compactness within the same cluster [30]. This index is an effective method to evaluate the clustering result and determine the optimal k. The Calinski-Harabasz index CH is defined as:

$$CH=\frac{\sum_{j=1}^{k}n_j\left\|\boldsymbol{\eta}_j-\bar{\boldsymbol{\eta}}\right\|_2^2}{\sum_{j=1}^{k}\sum_{\boldsymbol{g}_i\in\text{cluster }j}\left\|\boldsymbol{g}_i-\boldsymbol{\eta}_j\right\|_2^2}\cdot\frac{T_{\mathrm{an}}-k}{k-1} \tag{31}$$

where $\bar{\boldsymbol{\eta}}$ is the average value of the cluster centroids and n_j is the sample number of cluster j. The larger the value of CH, the greater the difference between different clusters and the greater the internal similarity within the same cluster. Therefore, when the value of CH peaks, the corresponding value of k is the optimal number of clusters.

IV. Solution Methodology

The above optimization model is a bi-level programming problem and the lower-level problem has nonconvex and nonlinear characteristics, so obtaining the optimal solution is difficult. To solve this problem, the original model is transformed into an MISOCP problem by SOC relaxation of the lower-level problem and primal-dual transformation.

A. SOCP Conversion for Lower-level Problem

To realize conic relaxation and reduce model complexity, the power flow equation is linearized as (52) in the Appendix. The power flow equation of the PQ bus and the slack bus can be expressed as:

$$P_{i,\phi}^{l}=\sum_{j=1}^{n_b}\sum_{\phi'=\mathrm{A,B,C}}\left(\Re_{j,\phi'}^{p,i,\phi}e_{j,\phi'}^{l}+\Im_{j,\phi'}^{p,i,\phi}f_{j,\phi'}^{l}\right)+\tilde{P}_{i,\phi} \tag{32}$$

$$Q_{i,\phi}^{l}=\sum_{j=1}^{n_b}\sum_{\phi'=\mathrm{A,B,C}}\left(\Re_{j,\phi'}^{q,i,\phi}e_{j,\phi'}^{l}+\Im_{j,\phi'}^{q,i,\phi}f_{j,\phi'}^{l}\right)+\tilde{Q}_{i,\phi} \tag{33}$$

$$P_{\mathrm{sub},\phi}^{l}=\sum_{j=1}^{n_b}\sum_{\phi'=\mathrm{A,B,C}}\left(\Re_{j,\phi'}^{p,\mathrm{sub},\phi}e_{j,\phi'}^{l}+\Im_{j,\phi'}^{p,\mathrm{sub},\phi}f_{j,\phi'}^{l}\right)+\tilde{P}_{\mathrm{sub},\phi} \tag{34}$$

$$Q_{\mathrm{sub},\phi}^{l}=\sum_{j=1}^{n_b}\sum_{\phi'=\mathrm{A,B,C}}\left(\Re_{j,\phi'}^{q,\mathrm{sub},\phi}e_{j,\phi'}^{l}+\Im_{j,\phi'}^{q,\mathrm{sub},\phi}f_{j,\phi'}^{l}\right)+\tilde{Q}_{\mathrm{sub},\phi} \tag{35}$$

Nonlinear constraints (5), (6), (22) and (24) can be formulated as the following SOC forms.

$$\sqrt{{P_{i,\phi,\mathrm{SOP}}^{l}}^{2}+{Q_{i,\phi,\mathrm{SOP}}^{l}}^{2}}\le P_{i,\phi,\mathrm{SOP}}^{\mathrm{L},l}/A_{i,\mathrm{SOP}} \tag{36}$$

$$\sqrt{{P_{j,\phi,\mathrm{SOP}}^{l}}^{2}+{Q_{j,\phi,\mathrm{SOP}}^{l}}^{2}}\le P_{j,\phi,\mathrm{SOP}}^{\mathrm{L},l}/A_{j,\mathrm{SOP}} \tag{37}$$

$$\left\|\begin{matrix}\left(e_{0,\mathrm{A}}^{1}-e_{1,\mathrm{A}}^{1}\right)\sqrt{r_{01,\mathrm{A}}T^{1}}/z_{01,\mathrm{A}}\\ \left(f_{0,\mathrm{A}}^{1}-f_{1,\mathrm{A}}^{1}\right)\sqrt{r_{01,\mathrm{A}}T^{1}}/z_{01,\mathrm{A}}\\ \vdots\\ \left[f_{n_b-1,\mathrm{C}}^{K_T}-f_{n_b,\mathrm{C}}^{K_T}\right]\sqrt{r_{n_b-1n_b,\mathrm{C}}T^{K_T}}/z_{n_b-1n_b,\mathrm{C}}\end{matrix}\right\|_2\le\sqrt{T_{\mathrm{an}}}\,f_{\mathrm{line}} \tag{38}$$

$$e_{i,\mathrm{un}}^{l}=1/3e_{i,\mathrm{A}}^{l}-1/6e_{i,\mathrm{B}}^{l}+\sqrt{3}/6f_{i,\mathrm{B}}^{l}-1/6e_{i,\mathrm{C}}^{l}-\sqrt{3}/6f_{i,\mathrm{C}}^{l} \tag{39}$$

$$f_{i,\mathrm{un}}^{l}=1/3f_{i,\mathrm{A}}^{l}-\sqrt{3}/6e_{i,\mathrm{B}}^{l}-1/6f_{i,\mathrm{B}}^{l}+\sqrt{3}/6e_{i,\mathrm{C}}^{l}-1/6f_{i,\mathrm{C}}^{l} \tag{40}$$

$$\left\|\left[e_{1,\mathrm{un}}^{1}\sqrt{T^{1}}\quad f_{1,\mathrm{un}}^{1}\sqrt{T^{1}}\quad\cdots\quad f_{n_b,\mathrm{un}}^{K_T}\sqrt{T^{K_T}}\right]^{T}\right\|_2\le\sqrt{T_{\mathrm{an}}}\,f_{\mathrm{U}} \tag{41}$$

Constraint (36) provides a lower bound for $P_{i,\phi\mathrm{SOP}}^{\mathrm{L},t}$, and then $P_{i,\phi\mathrm{SOP}}^{\mathrm{L},t}$ in the objective function is minimized, which helps constraint (36) converge to (5). The other constraints are similar to (5).

The voltage upper limit constraint in (28) and branch current constraint (30) can be converted to SOCP forms as (42) and (44) by replacing the voltage $U_{i,\phi}^{l}$ by its real part $e_{i,\phi}^{l}$ and imaginary part $f_{i,\phi}^{l}$. The voltage lower limit bound in (28) is converted to the SOC form (43) by introducing the rated voltage.

$$\sqrt{{e_{i,\phi}^{l}}^{2}+{f_{i,\phi}^{l}}^{2}} \le U^{\max} \tag{42}$$

$$\sqrt{\left(e_{i,\phi}^{l}-e_{i,\phi}^{r}\right)^{2}+\left(f_{i,\phi}^{l}-f_{i,\phi}^{r}\right)^{2}} \le U_{i,\phi}^{r}-U^{\min} \tag{43}$$

$$\sqrt{\left(e_{i,\phi}^{l}-e_{j,\phi}^{l}\right)^{2}+\left(f_{i,\phi}^{l}-f_{j,\phi}^{l}\right)^{2}} \le z_{ij,\phi}I_{ij,\phi}^{\max} \tag{44}$$

To avoid dispensable repetition, the upper and lower problems of the model are expressed in compact form:

Upper level

$$\min F_{\mathrm{UL}} = \boldsymbol{c}^{T}\boldsymbol{x}_{\mathrm{UL}} + \boldsymbol{d}^{T}\boldsymbol{x}_{\mathrm{PLL}} \tag{45a}$$

$$\boldsymbol{x}_{\mathrm{UL}} = \{0,1\} \tag{45b}$$

$$\boldsymbol{A}\boldsymbol{x}_{\mathrm{UL}} \le \boldsymbol{g} \tag{45c}$$

Lower level

$$\min F_{\mathrm{PLL}} = \boldsymbol{h}^{T}\boldsymbol{x}_{\mathrm{PLL}} \tag{46a}$$

$$\boldsymbol{B}\boldsymbol{x}_{\mathrm{PLL}} = \boldsymbol{j} \tag{46b}$$

$$\boldsymbol{C}\boldsymbol{x}_{\mathrm{PLL}} + \boldsymbol{D}\boldsymbol{x}_{\mathrm{UL}} \le \boldsymbol{l} \tag{46c}$$

$$\left\|\boldsymbol{E}_{i}\boldsymbol{x}_{\mathrm{PLL}} + \boldsymbol{s}_{i}\right\|_{2} \le \boldsymbol{v}_{i}^{T}\boldsymbol{x}_{PLL} + \boldsymbol{w}_{i}^{T}\boldsymbol{x}_{\mathrm{UL}} + z_{i}, i = 1,2,\cdots,n \tag{46d}$$

where (45a) is the objective function (11) of the upper-level problem; (45b) represents the variable of the upper-level problem as a binary variable; (45c) is the set of constraints (17) -(20); (46a) is the objective function of the lower-level problem (21); (46b) is the set of constraints (4), (23), (25), (26), (32) -(35), (39), and (40); (46c) is the set of constraints (1), (2), (7), and (8); and (46d) is the set of constraints (3), (9), (10), (29), (36)-(38), and (41) -(44).

B. Dual Lower-level Problem

Lagrangian duality theory [20] is used to transform the SOCP model of the lower-level problem into its dual model, which has the same optimal value as the primal model. The Lagrange dual function is formulated below:

$$\begin{aligned}\max \boldsymbol{F}_{\mathrm{DLL}} = &-\boldsymbol{j}^{T}\boldsymbol{\pi}_{1} - \boldsymbol{l}^{T}\boldsymbol{\pi}_{2} + \left(\boldsymbol{D}\boldsymbol{x}_{\mathrm{UL}}\right)^{T}\boldsymbol{\pi}_{2} \\ &-\sum_{i=1}^{n}\left[\boldsymbol{s}_{i}^{T}\boldsymbol{\mu}_{i} + \left(\boldsymbol{w}_{i}^{T}\boldsymbol{x}_{\mathrm{UL}} + z_{i}\right)\lambda_{i}\right]\end{aligned} \tag{47a}$$

$$\boldsymbol{B}^{T}\boldsymbol{\pi}_{1} + \boldsymbol{C}^{T}\boldsymbol{\pi}_{2} + \sum_{i=1}^{n}\boldsymbol{E}_{i}^{T}\boldsymbol{\mu}_{i} - \boldsymbol{h} = 0 \tag{47b}$$

$$\left\|\boldsymbol{\mu}_{i}\right\|_{2} \le \lambda_{i} \tag{47c}$$

$$\boldsymbol{\pi}_{2} \ge 0 \tag{47d}$$

where $\boldsymbol{\pi}_1$ and $\boldsymbol{\pi}_2$ are the Lagrangian multipliers of (46b) and (46c) and $\boldsymbol{\mu}_i$ and λ_i are the Lagrangian multipliers of (46d). $(\boldsymbol{D}\boldsymbol{x}_{\mathrm{UL}})^{T}\boldsymbol{\pi}_2$ and $\boldsymbol{w}_i^{T}\boldsymbol{x}_{\mathrm{UL}}\lambda_i$ in the objective function are the nonlinear terms, which can be transformed to mixed integer linear forms by the big-M method [31]. Taking $(\boldsymbol{D}\boldsymbol{x}_{\mathrm{UL}})^{T}\boldsymbol{\pi}_2$ as an example, the bilinear terms can be expressed as:

$$\left(\boldsymbol{D}\boldsymbol{x}_{\mathrm{UL}}\right)^{T}\boldsymbol{\pi}_{2} = \sum_{i=1}^{D_{row}}\sum_{j=1}^{D_{col}} x_{\mathrm{UL},i}\boldsymbol{D}_{i,j}^{T}\pi_{2,j} = \sum_{i=1}^{D_{row}}\sum_{j=1}^{D_{col}}\boldsymbol{D}_{i,j}^{T}\sigma_{i,j} \tag{48}$$

$$-Mx_{\mathrm{UL},i} \le \sigma_{i,j} \le Mx_{\mathrm{UL},i} \tag{49}$$

$$-M\left(1-x_{\mathrm{UL},i}\right) + \pi_{2,j} \le \sigma_{i,j} \le M\left(1-x_{\mathrm{UL},i}\right) + \pi_{2,j} \tag{50}$$

where D_{row} and D_{col} are respectively the row and column of $\boldsymbol{D}$. M is a sufficiently large number and $\sigma_{i,j}$ is an intermediate variable.

C. Single-level Equivalent

According to strong duality theory of conic optimization [20], (44a) is equal to (45a), namely,

$$F_{\mathrm{PLL}} = F_{\mathrm{DLL}} \tag{51}$$

The single-level equivalent can be obtained by combining the constraints of the primal lower-level problem, dual model, and strong duality. The single-level equivalent is formulated as a minimization of (45a) subject to (45b), (45c), (46b) -(46d), (47b) -(47d), and (48) -(51).

The single-level optimization model is a MISOCP problem by convex relaxation and linearization, and this model can be efficiently solved by commercial solvers.

V. Case Study

To verify the feasibility of the optimization model under the condition of different distribution network scales, IEEE 33-node and TPC test systems are used for case studies [21, 22]. The simulation program is tested on the MATLAB R2016b-YALMIP platform [32], and the MISOCP model is solved by the widely-used commercial solver MOSEK [33]. The hardware device is a computer with a 2.7 GHz Intel Core i7-7500 processor and 8 GB of RAM.

A. Parameter Settings

Annual hourly wind speed data from Texas, USA are used as the raw data [34], and wind power can be obtained using the function of wind speed to wind power [35]. The cut-in, rated, and cut-out wind speed of each wind turbine are assumed to be 3, 12, and 20 m/s, respectively. Hourly load data are generated using HOMER Pro software, which creates realistic-looking load data by setting random variability [10, 36]. Then, annual hourly wind power and load data are represented by per-unit (relative to the peak value). To determine the optimal number of clusters, we calculate *CH* values that gradually increase the number of clusters from 2 to 93 as shown in Fig. 3; when *k* is equal to 10, *CH* is the largest. Load and wind power scenarios with 10 clusters are shown in Table I.

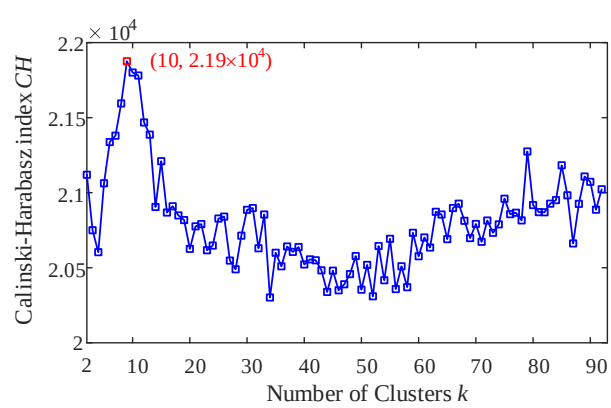

Fig. 3 Calinski-Harabasz index for each number of clusters

TABLE I
LOAD AND WIND POWER SCENARIOS

Scenario	Load (p.u.)	Wind Power (p.u.)	T^l (h)
1	0.4914	0.7359	1362
2	0.4951	0.9506	1445
3	0.6268	0.0491	882
4	0.5120	0.5041	1100
5	0.8172	0.0566	562
6	0.6772	0.9066	514
7	0.5069	0.2719	718
8	0.7377	0.3445	837
9	0.7033	0.6528	876
10	0.4863	0.0359	464

The load and DG power in Scenarios 2 and 5 represent two extreme conditions. As illustrated in Table I, load/wind power in Scenario 2 is the minimum, while Scenario 5 is the opposite. Settings of some other crucial parameters are shown in Table II.

TABLE II
SETTINGS OF SOME CRUCIAL PARAMETERS

Parameter	Value	Parameter	Value
$c_{I,DG}$ (RMB·kVA^{-1})	9000	d	0.08
$c_{I,SOP}$ (RMB·kVA^{-1})	2000	y (year)	20
$c_{O,DG}$ (RMB·kWh^{-1})	0.28	ς^{min}, ς^{max}	-0.8, 0.8
c_P (RMB·kWh^{-1})	0.54	ξ^{min}, ξ^{max}	-0.8, 0.8
α	0.01	$A_{i,SOP}$, $A_{j,SOP}$	0.02, 0.02
s_{DG} (kVA)	50	U^{min}, U^{max} (p.u.)	0.95, 1.05
s_{SOP} (kVA)	50	$I_{ij,\phi}^{max}$ (p.u.)	1.0

The pairwise comparison matrix data are shown in Table III, so the weighting coefficients of each sub-function are 0.42, 0.31, and 0.27, respectively, according to the algorithm in [27].

TABLE III
PAIRWISE COMPARISON MATRIX OF EACH SUB-OBJECTIVE FUNCTION

Sub-objective function	f_{line}	f_{SOP}	f_U
f_{line}	1	7/5	3/2
f_{SOP}	5/7	1	6/5
f_U	2/3	5/6	1

B. IEEE 33-node Test System

The IEEE 33-node test system shown in Fig. 4 has a rated voltage of 12.66 kV. Branch impedance and load parameters can be found in [21]. We assume that the load in [21] is the nominal value and the peak load in the hourly historical load is 1.3 times the nominal load. The loads of phases A, B, and C are 39, 31, and 30% of the total load, respectively. The location of DG is first affected by geographical and environmental factors, while other constraints such as power loss, voltage level, and density of DG units should also be comprehensively considered [35]. In this case, the candidate nodes for the installation of DG are nodes 6, 7, 13, 20, 23, 25, 29, and 30. The five normally open switches 7-20, 8-14, 11-21, 17-32, and 24-28 are candidate SOP installation sites. The capacity limits of each candidate DG or SOP site are 500 kVA. Four different cases are studied to verify the effectiveness of the proposed model.

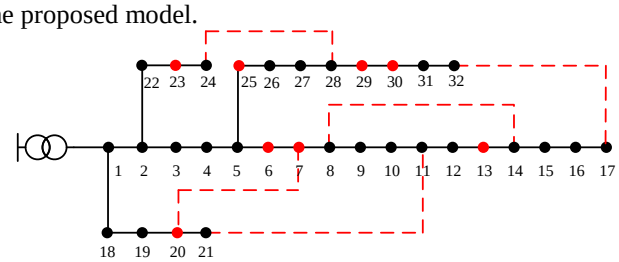

Fig.4 IEEE 33-node test system

Case 1: Without DG and SOPs.

Case 2: The power factor of a DG is unity, and the values of each phase power of an SOP are equal.

Case 3: Active and reactive power of DG and SOPs can be regulated, and the values of each phase power are equal.

Case 4: Each phase power of DG and SOPs can be regulated with individual phase control.

TABLE IV
DG PLANNING RESULTS IN THE IEEE 33-NODE SYSTEM

Location	Capacity (kVA)		
	Case 2	Case 3	Case 4
6	0	500	500
7	0	250	300
13	500	500	500
23	0	50	0
29	500	500	500
30	500	500	500
Total	1,500	2,300	2,300

TABLE V
SOP PLANNING RESULTS IN THE IEEE 33-NODE SYSTEM

Location	Capacity (kVA)		
	Case 2	Case 3	Case 4
7-20	500	300	300
8-14	100	0	0
11-21	500	500	500
17-32	500	50	50
24-28	500	500	500
Total	2,100	1,350	1,350

Detailed DG and SOP planning results are shown in Table IV and V, and only the nodes selected for installation are shown. In Case 2, the total DG and SOP capacities are 1500 and 2100 kVA, respectively, while the DG capacity in Cases 3 and 4 is 800 kVA more and the SOP capacity is 750 kVA less than in Case 2. Because DG cannot regulate reactive power in Case 2 and the candidate installation nodes 6 and 7 are also closed to the substation, the upper voltage constraint limits the planning of DG. More SOP units need to be installed to regulate reactive power and improve the voltage profile in Case 2. When the active and reactive power of DG can be regulated in Cases 3 and 4, less SOP capacity is installed. For instance, though the capacity of SOP 17-32 in Case 3 and 4 is only 50 kVA, the reactive power provided by the DGs at nodes 13, 29 and 30 improves the voltage profile. Moreover, although the DG capacity in Cases 3 and 4 is the same, the individual phase power control abilities of the DG and SOP units affect the installation location of the DG. The planning results of the upper-level problem further affect the objectives in the lower-level model, as shown in Table VI.

TABLE VI
COSTS, POWER LOSS, AND VOLTAGE UNBALANCE RESULTS IN THE IEEE 33-NODE SYSTEM

Case	$C_{I,DG}$ (RMB)	$C_{I,SOP}$ (RMB)	$C_{O,DG}$ (RMB)	$C_{O,SOP}$ (RMB)
Case 1	—	—	—	—
Case 2	1,375,650	427,980	1,445,492	42,000
Case 3	2,109,330	275,130	2,216,421	27,000
Case 4	2,109,330	275,130	2,216,421	27,000
Case	C_P (RMB)	Total (RMB)	Power loss (kW)	f_u (V)
Case 1	15,773,804	15,773,804	95.63	174..37
Case 2	10,322,363	13,613,485	37.17	111.85
Case 3	8,800,538	13,428,419	23.68	111.85
Case 4	8,785,023	13,412,904	20.46	72.94

The objective values in the upper and lower levels are shown in Table VI. In Case 1, the total cost is the electricity purchase cost from the upstream grid. When the DG and SOP units are installed, the investment and operation cost increase but the electricity purchase cost is greatly reduced, so the total cost is obviously reduced in Cases 2-4. As the DG capacity in Cases 3 and 4 is larger than in Case 2, the power purchase cost is lower. Especially in Case 4, each phase power of DG and SOP units can be controlled independently, which helps balance the load between the feeders of the same phase and reduce power loss as much as possible. So, the electricity purchase cost is reduced and the total cost of Case 4 is lower than for Case 3. Table VI also shows that Case 4 has the lowest power loss. In addition, when the DG and SOP units are installed, the voltage unbalance is significantly improved. Although each phase power of DG and SOP units in Cases 2 and 3 cannot be independently regulated, it can alleviate the unbalance of three-phase power to some extent. But in Case 4, the individual phase active and reactive power regulating ability of the DG and SOP units helps to significantly reduce the voltage unbalance problem of UDNs.

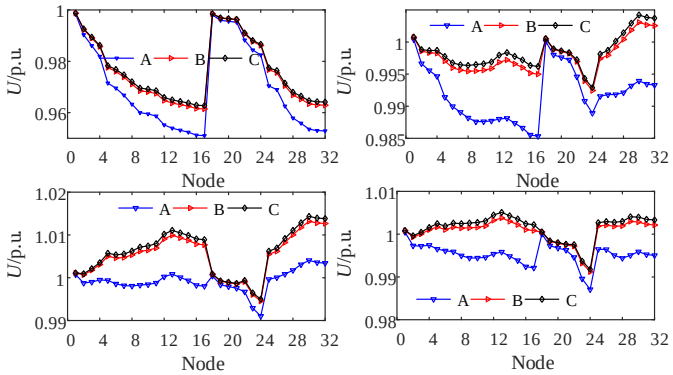

Fig. 5 Voltage profile of IEEE 33-node system for Cases1-4 in Scenario 2.

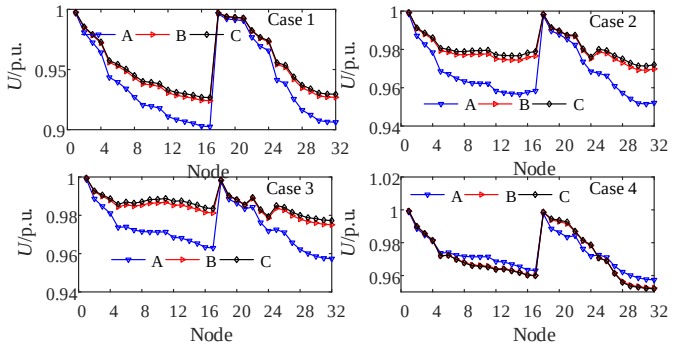

Fig. 6 Voltage profile of IEEE 33-node system for Cases 1-4 in Scenario 5.

As mentioned in Section V-A, Scenarios 2 and 5 represent two extreme conditions. Figs. 5-7 illustrate the voltage profile and voltage negative unbalance degree of the UDN in Scenarios 2 and 5, respectively.

In Scenario 2, the minimum voltage in all cases is over 0.95 because of the low load and high DG power generation. Even the voltage in part of the nodes is over 1 p.u. in Cases 2-4. However, in Scenario 5, when DG and SOP units are not installed, the minimum voltage of phase-A of the UDN in Scenario 5 is 0.9 p.u. But, the voltage profiles are improved and the minimum voltage is over 0.95 p.u. in Cases 2-4 in Scenario 5 due to the power control abilities of the DG and SOP units. Moreover, the voltage profile of phase-A, phase-B and phase-C are closer in Case 4, which indicates the voltage unbalance is better than in the other three cases.

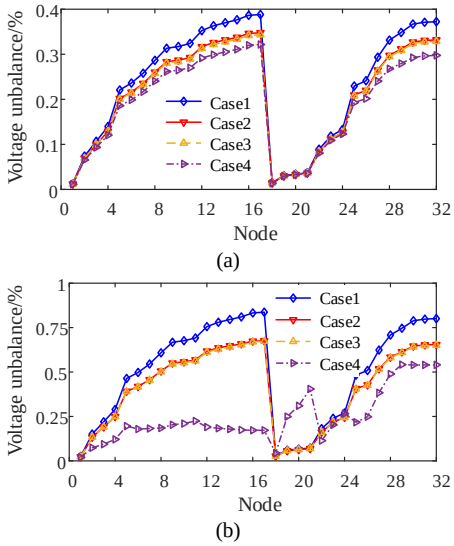

Fig. 7 Negative voltage unbalance degree of IEEE 33-node system for Cases 1-4: (a) Scenario 2; (b) Scenario 5.

Fig. 7 shows the voltage unbalance profile in Scenarios 2 and 5. In Scenario 2, the three-phase power unbalance is small during the low load period and peak DG generation, so the voltage unbalance improvement in Cases 2-4 is not obvious. But in Scenario 5, the voltage unbalance is significantly reduced in Case 4, though the voltage unbalance is slightly higher than the other three cases in nodes 18-22. In Case 2, DG injects active power into the UDN, and SOPs transfers active load and provide reactive power compensation; these actions help to reduce the load unbalance and improve voltage. Therefore, the voltage unbalance in Case 2 is improved compared to that of Case 1. Although more DGs are installed in Case 3 and DG units have reactive power compensation capability, the voltage unbalance is similar to Case 2 because the SOP capacity is larger in Case 2 than Case 3. In Case 4, the individual phase power control helps to minimize the voltage unbalance.

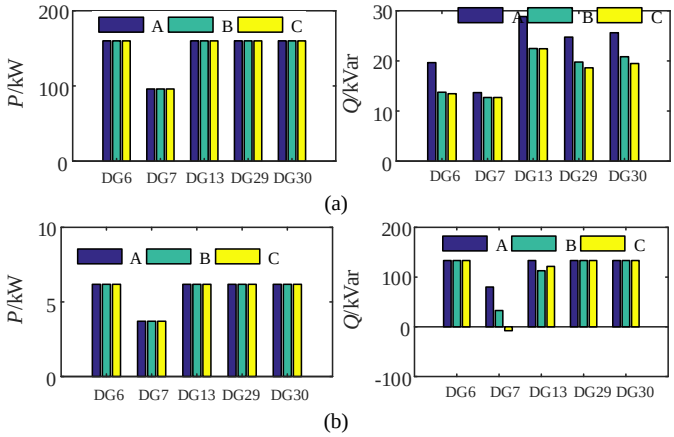

Fig. 8 Active and reactive power of DG units in the IEEE-33 node system: (a) Scenario 2; (b) Scenario 5.

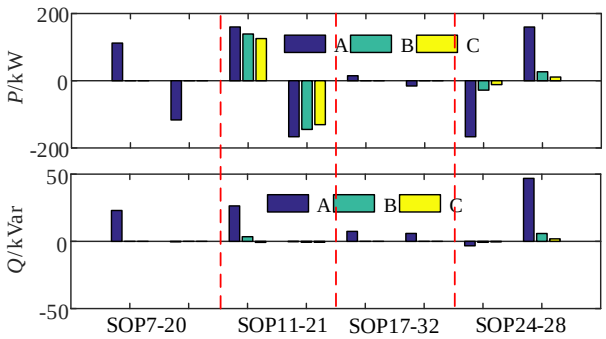

Fig. 9 Active and reactive power of SOPs in the IEEE-33 node system in Scenario 5.

To analyze the individual phase power regulation characteristics of DG and SOP units, the active and reactive power of the DG and SOP units in Case 4 for Scenarios 2 and 5 are shown in Figs. 8 and 9, respectively. For DG, the active power in each phase is the same but the reactive power is different. In fact, the active power output is the same as the maximum active power output. This is because only the maximum active power output of DG can reduce the power purchase cost in a UDN. In the peak load period, DG generates reactive voltage to improve the voltage in Scenario 5 as much as possible. The voltage unbalance is then adjusted by SOPs. SOPs improve the voltage and its unbalance by transferring active load and compensating reactive power. In Scenario 2, due to the low load, reactive power compensation and unbalanced compensation only rely on DG; the SOP power is close to 0, so the associated power bar chart is not given.

C. TPC Test System

The TPC test system is shown in Fig. 10, and its rated voltage is 11.4 kV. System parameters are provided in [22]. We also assume the peak load is 1.3 times the load in [22]. The load proportion of each phase is the same as the IEEE 33-node test system. The candidate installation nodes for DG are nodes 3, 7, 9, 10, 12, 17, 21, 23, 26, 28, 31, 33, 36, 39, 42, 45, 50, 53, 57, 59, 61, 64, 66, 68, 71, 75, 79, 82, and 83. The normally open switches 5-55, 7-60, 11-43, 12-72, 13-76, 14-18, 16-26, 20-83, 28-32, 29-39, 36-46, 40-42, and 53-64 are candidate SOP installation sites. The capacity limits of each candidate DG or SOP site are 1200 kVA. The four cases noted above are also used to verify the effectiveness of the proposed model on this larger distribution system.

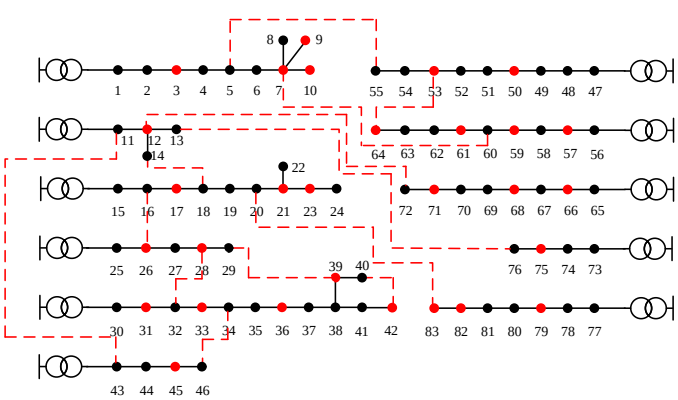

Fig. 10 TPC test system.

TABLE VII
DG PLANNING RESULTS IN THE TPC SYSTEM

Location	Capacity (kVA)			Location	Capacity (kVA)		
	Case 2	Case 3	Case 4		Case 2	Case 3	Case 4
3	50	50	50	45	50	50	50
7	1,100	850	1000	50	50	50	50
9	1,200	1200	1200	53	50	500	500
10	1,150	550	450	57	50	50	50
12	50	50	50	59	50	50	50
17	50	50	50	61	50	50	50
21	50	50	50	64	750	850	850
23	50	50	50	66	50	50	50
26	50	50	50	68	50	950	950
28	50	50	50	71	50	1200	1200
31	50	50	50	75	50	50	50
33	50	50	50	79	50	50	50
36	50	50	50	82	50	750	750
39	50	50	50	83	50	1200	1200
42	50	100	100	Total	5,450	9,100	9,150

TABLE VIII
SOP PLANNING RESULTS IN THE TPC SYSTEM

Location	Capacity (kVA)		
	Case 2	Case 3	Case 4
5-55	1150	450	450
7-60	1200	800	800
12-72	1050	300	300
20-83	1150	450	450
40-42	50	0	0
53-64	50	50	0
Total	4,650	2,050	2,000

The DG and SOP planning results in the TPC system are shown in Tables VII and VIII. The DG capacity in Cases 2-4 is 5,450, 9,100 and 9,150 kVA, respectively. The SOP capacity in Cases 2-4 is 4,650, 2,050, and 2,000 kVA, respectively. These results show Case 4 has a greater capacity to integrate more DG units. In Case 2, the UDN must install more SOP capacity to improve the voltage because DG cannot generate reactive power. The DG and SOP capacities in Case 3 are similar to those in Case 4.

TABLE IX
TOTAL COST, POWER LOSS, AND VOLTAGE UNBALANCE RESULTS IN THE TPC SYSTEM

Case	Total cost (RMB)	Power loss (kW)	f_u (V)
Case 1	111,947,301	253.06	150.83
Case 2	93,859,642	124.84	97.07
Case 3	93,268,423	73.82	97.07
Case 4	93,261,921	72.91	24.85

The total cost, power loss, and voltage unbalance results in the TPC system are given in Table IX. Due to the installation of DG and SOP units, Cases 2-4 are significantly better compared to Case 1. Moreover, the individual phase power control ability of DG and SOP units in Case 4 makes each objective optimal.

D. Algorithm Performance

SOP loss equation constraints (5) and (6), line loss equation constraint (22), and unbalance equation constraint (24) are relaxed in the MISOCP model. The relaxation gap is used to evaluate the accuracy of the SOCP relaxation [25]. Fig. 8 shows the relaxation gap $\Delta P_{\mathrm{SOP}}^{\mathrm{L}}$ of the SOP loss equation constraints for the IEEE 33-node and TPC systems. Each point represents the relaxation gap of each phase power loss of all VSCs. Relaxation gaps of line power loss and unbalance

equation constraints in the IEEE 33-node system are 3.8×10^{-11} and 0, respectively. Corresponding values in the TPC system are 8.3×10^{-4} and 1.7×10^{-4}. Fig. 11 is the boxplot for the relaxation gap of SOP loss equation constraints in all scenarios. The relaxation gap values are all on the order of 10^{-7}, which are small enough that SOCP relaxation is considered valid.

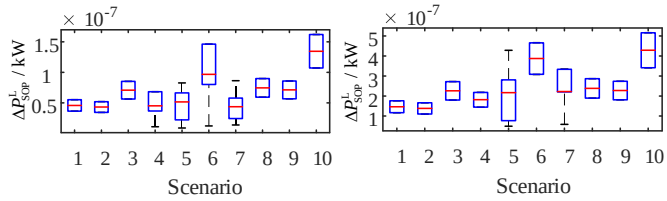

Fig. 11 Relaxation gap values of SOP loss equation constraints: (a) IEEE 33-node system; (b) TPC system.

Power flow equation constraint (30) is linearized, and will cause a voltage error between the approximate and accurate values of voltage. Fig. 12 shows the absolute value of each phase voltage error of all nodes in all scenarios, the maximum of which is no more than 3×10^{-3} p.u. Therefore, the power flow linearization is effective.

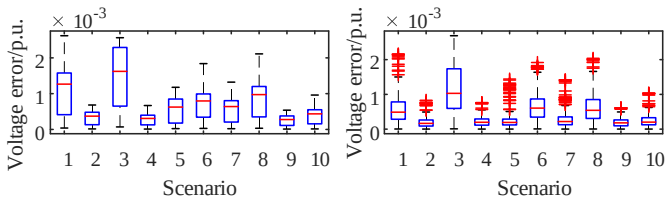

Fig. 12 Voltage error caused by power flow linearization: (a) IEEE 33-node system; (b) TPC system.

TABLE X
COMPARISON OF SOLVING EFFICIENCY AND CONVERGENCE

Test system	Case	Time (s)		Total Cost (RMB)	
		MINLP	MISOCP	MINLP	MISOCP
IEEE 33-node	2	714	35	13,665,209	13,613,485
	3	768	39	13,490,692	13,428,419
	4	688	23	13,478,320	13,412,904
TPC	2	—	218	—	93,859,642
	3	—	207	—	93,268,423
	4	—	214	—	93,261,921

The solving efficiency and convergence of the proposed MISOCP and original MINLP models are shown in Table X. The MINLP model is solved by genetic algorithm and the IPOPT solver [16, 37]. The computing time of the MISOCP model in the IEEE 33-node system is no more than 40 s, while the MINLP model is more than 680 s. The total cost determined by the MINLP model is also more than that determined by the MISOCP model. In addition, the MINLP model cannot converge in the TPC system but the proposed MISOCP model can obtain the optimal solution. This is because the original problem is nonconvex, making it difficult to obtain an optimal solution.

VI. CONCLUSION

This paper proposes a bi-level optimization for DG and SOP planning that incorporates their individual phase power control in UDNs. The upper-level model is the optimal placement and sizing of DG and SOP units with a minimization of the total cost of the UDN, while the lower-level model considers the capability of DG and SOP units in terms of power loss reduction and voltage unbalance improvement.

The proposed bi-level model is transformed into a single-level MISOCP model using duality theory, SOC relaxation, and power flow linearization. This model is a convex optimization model, which can obtain fast and accurate solutions. The stochastic behavior of both load demand and renewable energy generation are represented by multiple scenarios based on annual hourly data and a clustering method.

The effectiveness and performance of the proposed model is validated by case studies. The results clearly show that active and reactive power regulation by DG and SOP units can increase the integrated capacity of DGs and reduce the total cost of the UDN. Moreover, individual phase power regulation of DG and SOP units can minimize the power loss, thus further reducing the electricity purchase cost and total cost of the UDN. This power regulation method can also significantly mitigate the voltage unbalance. The values of the SOC relaxation gap and errors of the linearization of power flow equations are within a reasonable range, and the convergence of the model is also improved. The proposed planning model can effectively incorporate the individual phase power control abilities of DG and SOP units, which can significantly improve the system operation in UDNs.

APPENDIX

The three-phase power flow equation is linearized as follows:

$$
\begin{aligned}
&P_{i,\phi}^{l}+\mathrm{j}Q_{i,\phi}^{l}\\
&=\dot{U}_{i,\phi}^{l}\dot{I}_{i,\phi}^{l\ *}=\dot{U}_{i,\phi}^{l}\sum_{j\in i}\sum_{\phi'=\mathrm{A,B,C}}y_{i,\phi j,\phi'}^{*}\dot{U}_{j,\phi'}^{l\ *}\\
&=\left(\dot{U}_{i,\phi}^{r}+\Delta\dot{U}_{i,\phi}^{l}\right)\sum_{j\in i}\sum_{\phi'=\mathrm{A,B,C}}y_{i,\phi j,\phi'}^{*}\left(\dot{U}_{j,\phi'}^{r}+\Delta\dot{U}_{j,\phi'}^{l}\right)^{*}\\
&=\dot{U}_{i,\phi}^{r}\sum_{j\in i}\sum_{\phi'=\mathrm{A,B,C}}y_{i,\phi j,\phi'}^{*}\dot{U}_{j,\phi'}^{r*}+\dot{U}_{i,\phi}^{r}\sum_{j\in i}\sum_{\phi'=\mathrm{A,B,C}}y_{i,\phi j,\phi'}^{*}\Delta\dot{U}_{j,\phi'}^{l\ *}\\
&\quad+\Delta\dot{U}_{i,\phi}^{l}\sum_{j\in i}\sum_{\phi'=\mathrm{A,B,C}}y_{i,\phi j,\phi'}^{*}\dot{U}_{j,\phi'}^{r*}+\Delta\dot{U}_{i,\phi}^{l}\sum_{j\in i}\sum_{\phi'=\mathrm{A,B,C}}y_{i,\phi j,\phi'}^{*}\Delta\dot{U}_{j,\phi'}^{l\ *}\\
&\approx\dot{U}_{i,\phi}^{r}\sum_{j\in i}\sum_{\phi'=\mathrm{A,B,C}}y_{i,\phi j,\phi'}^{*}\dot{U}_{j,\phi'}^{r*}+\dot{U}_{i,\phi}^{r}\sum_{j\in i}\sum_{\phi'=\mathrm{A,B,C}}y_{i,\phi j,\phi'}^{*}\left(\dot{U}_{j,\phi'}^{l}-\dot{U}_{j,\phi'}^{r}\right)^{*}\\
&\quad+\left(\dot{U}_{i,\phi}^{l}-\dot{U}_{i,\phi}^{r}\right)\sum_{j\in i}\sum_{\phi'=\mathrm{A,B,C}}y_{i,\phi j,\phi'}^{*}\dot{U}_{j,\phi'}^{r*}\\
&\approx-\dot{U}_{i,\phi}^{r}\sum_{j\in i}\sum_{\phi'=\mathrm{A,B,C}}y_{i,\phi j,\phi'}^{*}\dot{U}_{j,\phi'}^{r*}+\dot{U}_{i,\phi}^{r}\sum_{j\in i}\sum_{\phi'=\mathrm{A,B,C}}y_{i,\phi j,\phi'}^{*}\dot{U}_{j,\phi'}^{l\ *}\\
&\quad+\dot{U}_{i,\phi}^{l}\sum_{j\in i}\sum_{\phi'=\mathrm{A,B,C}}y_{i,\phi j,\phi'}^{*}\dot{U}_{j,\phi'}^{r*}\\
&\approx\left[\sum_{j=1}^{n_b}\sum_{\phi'=\mathrm{A,B,C}}\left(\Re_{j,\phi'}^{p,i,\phi}e_{j,\phi'}^{l}+\Im_{j,\phi'}^{p,i,\phi}f_{j,\phi'}^{l}\right)+\tilde{P}_{i,\phi}\right]+\\
&\quad\mathrm{j}\cdot\left[\sum_{j=1}^{n_b}\sum_{\phi'=\mathrm{A,B,C}}\left(\Re_{j,\phi'}^{q,i,\phi}e_{j,\phi'}^{l}+\Im_{j,\phi'}^{q,i,\phi}f_{j,\phi'}^{l}\right)+\tilde{Q}_{i,\phi}\right]
\end{aligned}
\tag{52}
$$

where $\dot{U}_{i,\phi}^{r}$ is the rated voltage, and it is assumed that all nodes have the same rated voltage, $\dot{U}_{i,\mathrm{A}}^{r}=\dot{U}^{r}$, $\dot{U}_{i,\mathrm{B}}^{r}=\dot{U}^{r}e^{-\mathrm{j}2\pi/3}$, $\dot{U}_{i,\mathrm{C}}^{r}=\dot{U}^{r}e^{-\mathrm{j}4\pi/3}$, and $\Delta\dot{U}_{i,\phi}^{l}=\dot{U}_{i,\phi}^{l}-\dot{U}_{i,\phi}^{r}$.

REFERENCES

[1] M. Sedghi, A. Ahmadian and M. Aliakbar-Golkar, "Optimal storage planning in active distribution network considering uncertainty of wind power distributed generation," *IEEE Trans. Power Syst*., vol. 31, no. 1, pp. 304-316, Jan. 2016.

[2] A. J. Valdberg and M. W. Dwyer, "Distribution resources plan rulemaking (R. 14-08-013) locational net benefit analysis working group final report," 2019. [Online]. Available: http://drpwg.org/wp-content/uploads/2016/07/R1408013-et-al-SCE-LNBA-Working-Group-Final-Report.pdf

[3] M. Bazrafshan, N. Gatsis and E. Dall'Anese, "Placement and sizing of inverter-based renewable systems in multi-phase distribution networks," *IEEE Trans. Power Syst.* vol. 34, no. 2, pp. 918-930, Mar. 2019.

[4] J. M. Bloemink and T. C. Green, "Increasing distributed generation penetration using soft normally-open points," *IEEE PES General Meeting*, Providence, RI, 2010, pp. 1-8.

[5] H. Ji, C. Wang, P. Li, F. Ding and J. Wu, "Robust operation of soft open points in active distribution networks with high penetration of photovoltaic integration," *IEEE Trans. Sustain. Energy*, vol. 10, no. 1, pp. 280-289, Jan. 2019.

[6] P. Li, H. Ji, C. Wang, J. Zhao, G. Song, F. Ding and J. Wu, "Coordinated control method of voltage and reactive power for active distribution networks based on soft open point," *IEEE Trans. Sustain.* Energy, vol. 8, no. 4, pp. 1430-1442, Oct. 2017.

[7] E. Prieto-Araujo, A. Junyent-Ferré, G. Clariana-Colet, and O. Gomis-Bellmunt, "Control of modular multilevel converters under singular unbalanced voltage conditions with equal positive and negative sequence components," *IEEE Trans. Power Syst*., vol. 32, pp. 2131-2141, May 2017.

[8] K. Ma, R. Li and F. Li, "Quantification of additional asset reinforcement cost from 3-phase imbalance," *IEEE Trans. Power Syst.*, vol. 31, no. 4, pp. 2885-2891, July 2016.

[9] S. M. Fazeli, H. W. Ping, N. Bin Abd Rahim and B. T. Ooi, "Individual-phase control of 3-phase 4-wire voltage-source converter," *IET Power Electron.*, vol. 7, no. 9, pp. 2354-2364, Sep. 2014.

[10] C. Zhang, J. Li, Y. J. Zhang and Z. Xu, "Optimal location planning of renewable distributed generation units in distribution networks: an analytical approach," *IEEE Trans. Power Syst.*, vol. 33, no. 3, pp. 2742-2753, May 2018.

[11] B. R. Pereira, G. R. M. da Costa, J. Contreras and J. R. S. Mantovani, "Optimal distributed generation and reactive power allocation in electrical distribution systems," *IEEE Trans. Sustain. Energy*, vol. 7, no. 3, pp. 975-984, Jul. 2016.

[12] H. Xing and X. Sun, "Distributed generation locating and sizing in active distribution network considering network reconfiguration," *IEEE Access*, vol. 5, pp. 14768-14774, Aug. 2017.

[13] Q. Li, R. Ayyanar and V. Vittal, "Convex optimization for DES planning and operation in radial distribution systems with high penetration of photovoltaic resources," *IEEE Trans. Sustain. Energy*, vol. 7, no. 3, pp. 985-995, Jul. 2016.

[14] S. S. AlKaabi, V. Khadkikar and H. H. Zeineldin, "Incorporating PV inverter control schemes for planning active distribution networks," *IEEE Trans. Sustain. Energy*, vol. 6, no. 4, pp. 1224-1233, Oct. 2015.

[15] C. Wang, G. Song, P. Li, H. Ji, J. Zhao, and J. Wu, "Optimal siting and sizing of soft open points in active electrical distribution networks," *Appl. Energy*, vol. 189, pp. 301-309, 2017.

[16] L. Zhang, C. Shen, Y. Chen, S. Huang, and W. Tang, "Coordinated allocation of distributed generation, capacitor banks and soft open points in active distribution networks considering dispatching results," *Appl. Energy*, vol. 231, pp. 1122-1131, 2018.

[17] M. M. Othman, W. El-Khattam, Y. G. Hegazy and A. Y. Abdelaziz, "Optimal placement and sizing of distributed generators in unbalanced distribution systems using supervised big bang-big crunch method," *IEEE Trans. Power Syst.*, vol. 30, no. 2, pp. 911-919, Mar. 2015.

[18] M. Asensio, G. Muñoz-Delgado and J. Contreras, "Bi-level approach to distribution network and renewable energy expansion planning considering demand response," *IEEE Trans. Power Syst.*, vol. 32, no. 6, pp. 4298-4309, Nov. 2017.

[19] J. M. Arroyo, "Bilevel programming applied to power system vulnerability analysis under multiple contingencies," *IET Gener. Transm. Distrib.*,vol. 4, no. 2, pp. 178–190, 2010.

[20] S. Boyd and L. Vandenberghe, Convex Optimization. Cambridge, U.K.:Cambridge Univ. Press, 2004

[21] M. E. Baran and F. F. Wu, "Network reconfiguration in distribution systems for loss reduction and load balancing," *IEEE Trans. Power Del*., vol. 4, no. 2, pp. 1401-1407, Apr. 1989

[22] C.T. Su and C.S. Lee, "Network reconfiguration of distribution systems using improved mixed-integer hybrid differential evolution," *IEEE Trans. Power Del.*, vol. 18, no. 3, pp. 1022-1027, Jul. 2003.

[23] Y. Zhang and C. Qu, "Table-based direct power control for three-phase ac/dc converters under unbalanced grid voltages," *IEEE Trans. Power Electron.*, vol. 30, no. 12, pp. 7090-7099, Dec. 2015.

[24] J. Wang, N. Zhou, Y. Ran and Q. Wang, "Optimal operation of active distribution network involving the unbalance and harmonic compensation of converter," *IEEE Trans. Smart Grid*. vol. 10, no. 5, pp. 5360-5373, Sep. 2019.

[25] P. Li, H. Ji, C. Wang, J. Zhao, G. Song, F. Ding and J. Wu., "Optimal operation of soft open points in active distribution networks under three-phase unbalanced conditions," *IEEE Trans. Smart Grid*, vol. 10, no. 1, pp. 380-391, Jan. 2019.

[26] M. Asensio, G. Muñoz-Delgado and J. Contreras, "Bi-level approach to distribution network and renewable energy expansion planning considering demand response," *IEEE Trans. Power Syst.*, vol. 32, no. 6, pp. 4298-4309, Nov. 2017.

[27] H. Wang, W. Zhang and Y. Liu, "A robust measurement placement method for active distribution system state estimation considering network reconfiguration," *IEEE Trans. Smart Grid*, vol. 9, no. 3, pp. 2108-2117, May 2018.

[28] M. Nick, R. Cherkaoui and M. Paolone, "Optimal allocation of dispersed energy storage systems in active distribution networks for energy balance and grid support," *IEEE Trans. Power Syst.*, vol. 29, no. 5, pp. 2300-2310, Sep. 2014.

[29] M. Kim and R.S. Ramakrishna, "New indices for cluster validity assessment," *Pattern Recognit. Lett*., vol. 26, no. 15, pp. 2353-2363, 2005.

[30] F. Khayatian, L. Sarto and G. Dall'O', "Building energy retrofit index for policy making and decision support at regional and national scales," *Appl. Energy*, vol. 206, pp. 1062-1075, 2017.

[31] S. Pineda and J. M. Morales, "Solving linear bilevel problems using big-Ms: not all that glitters is gold," *IEEE Trans. Power Syst*., vol. 34, no. 3, pp. 2469-2471, May 2019.

[32] J. Löfberg, "A toolbox for modeling and optimization in MATLAB," *in Proc. CACSD Conf.*, Taipei, Taiwan, 2004.

[33] The MOSEK optimization toolbox for MATLAB manual version 8.0. MOSE K ApS. [Online]. Available: https://www.mosek.com/downloads/list/8/

[34] ASOS Network. 2019 [Online]. Available: https://mesonet.agron.iastate.edu/request/download.phtml?network=TX_ASOS.

[35] Y. Gao, X. Hu, W. Yang, H. Liang and P. Li, "Multi-objective bilevel coordinated planning of distributed generation and distribution network frame based on multiscenario technique considering timing characteristics," *IEEE Trans. Sustain. Energy*, vol. 8, no. 4, pp. 1415-1429, Oct. 2017.

[36] Generating Synthetic Load Data. 2019 [Online]. Available: https://www.homerenergy.com/products/pro/docs/3.13/generating_synthetic_load_data.html.

[37] IPOPT. [Online]. Available at: https://projects.coinor.org/Ipopt.

Jian Wang (S'18) received the B.S. degree in electrical engineering from Chongqing University, Chongqing, China, in 2015. He is working toward the Ph.D. degree in electrical engineering in Chongqing University. From 2018 to 2019, He was a visiting research student at University of Saskatchewan, Saskatoon, SK, Canada. His research interests include power systems planning, operation and restoration.

Niancheng Zhou (M'18) received the B.S., M.S., and Ph.D. degrees in electrical engineering from Chongqing University, Chongqing, China, in 1991, 1994, and 1997, respectively. He worked at Chongqing Kuayue Technology Co, Ltd., from 1997 to 2003. From 2010 to 2011, he was a research fellow of Nanyang Technological University, Singapore.

He is currently a Professor in School of Electrical Engineering, Chongqing University, China. His research interests include analysis, operation of power system, microgrid and power quality.

C. Y. Chung (M'01-SM'07-F'16) received the B.Eng. (with First Class Honors) and Ph.D. degrees in electrical engineering from The Hong Kong Polytechnic University, Hong Kong, China, in 1995 and 1999, respectively.

He is currently a Professor, the NSERC/SaskPower (Senior) Industrial Research Chair in Smart Grid Technologies, and the SaskPower Chair in Power Systems Engineering with the Department of Electrical and Computer Engineering at the University of Saskatchewan, Saskatoon, SK, Canada.

Dr. Chung is an Editor of IEEE TRANSACTIONS ON POWER SYSTEMS, IEEE TRANSACTIONS ON SUSTAINABLE ENERGY, and IEEE POWER ENGINEERING LETTERS. He is also an IEEE PES Distinguished Lecturer and a Member-at Large (Global Outreach) of the IEEE PES Governing Board.

Qianggang Wang (S'13–M'15) received the B.S. and Ph.D. degrees in electrical engineering from Chongqing University, Chongqing, China, in 2009 and 2015, respectively. From 2015 to 2016 He was a research fellow of Nanyang Technological University, Singapore.

He is currently an Associate Professor with Chongqing University. His research interests include power system operation, microgrids, and power quality.